LBL-31064
Preprint

Lawrence Berkeley Laboratory
UNIVERSITY OF CALIFORNIA

Materials & Chemical Sciences Division

Submitted to Journal of Chemical Physics

Reaction Geometry from Orbital Alignment Dependence of Ion Pair Production in Crossed Beams $Ba(^1P_1)$-Br_2 Reactions

A.G. Suits, H. Hou, H.F. Davis, Y.T. Lee, and J.-M. Mestdagh

July 1991

Prepared for the U.S. Department of Energy under Contract Number DE-AC03-76SF00098

DISCLAIMER

LBL-31064

REACTION GEOMETRY FROM ORBITAL ALIGNMENT DEPENDENCE OF ION PAIR PRODUCTION IN CROSSED BEAMS $Ba(^1P_1)$-Br_2 REACTIONS

Arthur G. Suits, Hongtao Hou, H. Floyd Davis,
and Yuan T. Lee

Department of Chemistry
University of California
and
Chemical Sciences Division
Lawrence Berkeley Laboratory
Berkeley, CA 94720 USA

and

Jean-Michel Mestdagh

DRECAM/SPAM
CEN Saclay
91191 Gif-sur-Yvette Cedex, France

July 1991

This work was supported by the Director, Office of Energy Research, Office of Basic Energy Sciences, Chemical Sciences Division, of the U.S. Department of Energy under Contract No. DE-AC03-76SF00098.

Reaction Geometry from Orbital Alignment Dependence of Ion Pair Production in Crossed Beams $Ba(^1P_1)$-Br_2 Reactions

Arthur G. Suits, Hongtao Hou, H. Floyd Davis, and Yuan T. Lee
Chemical Sciences Division
Lawrence Berkeley Laboratory and
Department of Chemistry
University of California
Berkeley, CA 94720

and

Jean-Michel Mestdagh
DRECAM/SPAM
CEN Saclay
91191 Gif-sur-Yvette Cedex, France

Abstract

Strong orbital alignment dependence was observed for Ba^+ produced in crossed beams reaction of $Ba(^1P_1)$ with Br_2. The peak of this dependence varied strongly with scattering angle for alignment of the p orbital in the scattering plane, with the maximum flux seen for perpendicular alignment with respect to the relative velocity vector. The measured Ba^+ was always favored by alignment of the orbital in the scattering plane, regardless of laboratory scattering angle. The experimental results suggest that this charge transfer process is dominated by large impact parameter collisions which achieve collinear nuclear geometry and Σ orbital alignment at the crossing point. Orbital locking is probably not important owing to the large internuclear distance of the crossing region.

I. INTRODUCTION

A simple relation exists between impact parameter and scattering angle in atom-atom scattering, so angular distributions in crossed beams experiments have been used with considerable success to study the distance dependence of interatomic forces.[1-3] Extremely accurate interatomic potentials are now routinely obtained from elastic scattering results. For inelastic atom-molecule scattering there exists no simple correspondence between scattering angle and impact parameter owing mainly to the tremendous possible variation in scattering angle with collision geometry. Yet the differential cross sections still contain a wealth of information, and crossed beams experiments have been used to explore the anisotropy of the atom-molecule interaction potential directly in the differential cross section, as in the atom-atom experiments, and indirectly through such phenomena as rotational rainbows.[4-6] Reactive scattering represents the greatest challenge to the crossed beams technique because large numbers of states, even entirely different product channels, may be accessible. These may exhibit varying partitioning of the available energy between internal modes and translation, so there may not exist strong correlations between these quantities. The dynamics may thus be obscured by a broad and overlapping range of final state distributions. Nevertheless, scattering results often provide remarkable insight into the microscopic features of reactive collisions, particularly when translational energy distributions are also obtained, or when the reaction occurs by way of some constrained geometries[7] or shows distinctive

dynamic behavior.[8] In recent years it has become possible, through use of electrostatic focusing techniques, polarized narrow band lasers and related methods, to prepare oriented or aligned atomic and molecular reagents.[10-11] The use of such prepared reagents in crossed beams experiments provides a means of extending the power of crossed beams techniques to explore the full geometry of the collisional encounter.

For barium excited to the ($^1P_1$) electronic state, thermal energy collisions with halogen molecules can yield the ion pair Ba^+ and X_2^-. The use of a linearly polarized laser to prepare the electronically excited barium atoms allows for alignment of the excited state orbital with respect to the relative velocity vector, which is itself well-defined under crossed beams conditions. Because the electronic potential energy surfaces possess different symmetries depending on initial orbital alignment, branching into nonadiabatic reaction pathways may be strongly modulated by means of laser polarization.[12,13] Furthermore, this preparation of aligned reactants breaks the cylindrical symmetry which prevails in crossed beams experiments. For scattering dominated by orbital angular momentum, π^+ and π^- configurations may be defined with respect to the scattering plane.[14] In effect, the detector may act as a polarizer: in favorable cases we may distinguish products for which the initial nuclear and electronic orbital angular momentum vectors are either parallel or perpendicular. If the symmetries of the electronic wavefunctions are known for relevant states of the collision complex, the dependence of reaction cross section on initial orbital alignment may be used to infer the internuclear geometry at the critical configuration at which electron transfer occurs.

The study of collisions involving aligned orbitals has proceeded rapidly in recent years. As a result of pioneering studies by Pauly[15-17], Hertel[18-20], Leone[21-22] and others in the late 70's and early 80's, there now exist several "well-understood cases" in atom-atom scattering. In contrast alignment dependence in atom-molecule scattering, both inelastic[23,24] and reactive, has seldom been reported and is not as well understood. Earlier work in our laboratory described significant polarization effects for crossed beams reaction of Na(4D) with O_2.[25,26] Parallel alignment of the sodium d orbital with respect to the relative velocity vector led to efficient quenching via the ground state O_2^- ion. Formation of the reactive product, however, required a close collision from the covalent surface, and led to sharply backscattered NaO. In addition, the location of the peak in the polarization dependence changed with laboratory scattering angle, demonstrating the importance of a collinear nuclear geometry at the crossing point. In 1982 Rettner and Zare reported remarkable polarization effects on product state branching and cross sections in reaction of $Ca(^1P_1)$ with HCl and Cl_2 in a beam-gas experiment.[27] In the former reaction they found chemiluminescence from the CaCl(A $^2\Pi$) state enhanced by initial π orbital alignment, while the CaCl(B $^2\Sigma$) state was favored by Σ alignment. They attributed the dependence of final electronic state on initial orbital alignment to a preservation of the symmetry of the initially prepared state through the reactive encounter, with reaction initiated by transfer of the calcium s rather than p electron. In the Cl_2 reaction, however, all products were found to be favored by the π configuration. This was ascribed to an alignment dependence of the probability for transfer of the p electron at the outer crossing of the potential energy surfaces, with

reaction favored by broadside approach. These arguments have some bearing on the work presented here, and will be considered in detail in the ensuing discussion.

We previously reported strong orbital alignment dependence for Ba^+ produced from crossed beams reaction of $Ba(^1P_1)$ with Cl_2 at a collision energy of 3 eV.[28] This alignment dependence was only observed at back angles with respect to the barium beam, although unfavorable kinematics precluded viewing angles significantly forward of the center of mass. The analogous reaction with Br_2 was expected to show many of the same features as the Cl_2 reaction, while the kinematics are considerably more favorable. The alignment dependence for Ba^+ produced from reaction of $Ba(^1P_1)$ with Br_2 was found to be strongly dependent on laboratory scattering angle, and different dependence was observed for in-plane and out-of-plane rotation of the orbital. All observations can be reconciled by a mechanism in which large impact parameter collisions dominate in long-range electron-transfer of those collisions which achieve a Σ configuration (in the molecular reference frame) at the crossing seam.

II. EXPERIMENTAL

The crossed beams apparatus, which has been described in detail previously,[29,30] has been modified for the detection of chemiions. A supersonic barium beam was formed by expanding a mixture of barium and neon (~5%) from the nozzle of a resistively heated one-piece molybdenum oven assembly to be described in detail in a forthcoming publication.[31] Under typical operating conditions, the nozzle was ~1500°C

(corrected optical pyrometer reading), while the barium reservoir was maintained about 400° cooler. An auxiliary radiative graphite heating element surrounding the barium reservoir allowed its temperature to be adjusted independently of the nozzle. The barium beam passed through a heated molybdenum skimmer and a collimating slit, then to a collision chamber maintained at ~10^{-7} Torr. The bromine beam was produced by expanding a 3% Br_2/He mixture through a 0.075 mm nozzle heated to 200°C. The bromine beam passed through a skimmer and collimating slit to cross the barium beam at 90° in the collision chamber, yielding an interaction volume of 8 mm^3.

The interaction region of the collision chamber was surrounded by a stainless steel electrode, shown in Figure 1A, maintained field-free 120V above ground. Ions produced in the reaction were allowed to pass through an aperture in the field-free region and accelerated to ground potential at the entrance to a quadrupole mass spectrometer through focusing lenses and a retarding electrode. Mass selected ions were counted by means of a Daly detector and associated electronics. The entire detector assembly could be rotated in the plane of the two beams, allowing for measurement of product flux as a function of laboratory scattering angle. The retarding potential, gating and scalers were controlled by computer.

Electronically excited barium atoms were prepared by optical pumping at the interaction region by means of a single-frequency ring dye laser tuned to the Ba(^{1}S-^{1}P) transition at 554 nm. Metastable D states are also populated by radiative decay from the P state, and the ^{138}Ba composition of the beam is estimated to be ~35% ground state Ba, ~35% Ba(^{1}P) and 30% Ba(^{1,3}D). All other isotopes (29%) remain in the ground state. In

the present study at 1.6 eV collision energy, no reaction yielding Ba^+ is energetically possible from the ground state. The contribution from the metastable D states, estimated by exciting upstream of the interaction region, was found to be negligible. The measured Ba^+ comes almost entirely from $Ba(^1P_1)$. The laser polarization was rotated by means of a double Fresnel rhomb driven by a stepper motor. The laser beam was directed perpendicular to the plane of the beams for the in-plane polarization rotation experiments (figure 1B), or collinear with the bromine beam (figure 1C) for the out-of-plane polarization rotation experiments. The fluorescence from the $Ba(^1P_1$-$^1S_0)$ transition was directed through a telescope onto a photomultiplier tube and recorded along with the data in both geometries. The anisotropy of this fluorescence confirmed virtually complete alignment of the $Ba(^1P_1)$ state.

III. RESULTS

The charge transfer reaction of $Ba(^1P_1)$ with Br_2 at 1.6 eV collision energy was studied as a function of orbital alignment and laboratory scattering angle for both in-plane and out-of-plane rotation of the barium p orbital. ß, the angle between the relative velocity vector and the laser polarization, is taken to be in the positive direction for clockwise rotation of the orbital viewed from above, schematically illustrated in Figure 2A. For out-of-plane rotation the polarization angle, θ, is defined with respect to a vertical line through the scattering plane (Figure 2B). The positive sense of polarization rotation is taken to be clockwise when viewing into the bromine beam. As

can be seen in Figure 2B, because the laser is not perpendicular to the relative velocity vector, parallel orbital alignment (ß=0°) cannot be achieved in this experimental geometry. For the out-of-plane rotation experiments the orbital alignment varies from perpendicular to the relative velocity vector (ß=90°) at θ = 0°, to a minimum (ß=35°) for in-plane (θ = 90°) alignment.

A. In-Plane Polarization Rotation

Figure 3 shows laboratory angular distributions of Ba^+ taken with parallel (ß=0°) perpendicular (ß=90°) and ß = ±45° alignment for in-plane rotation of the orbital. All polarizations showed forward or forward-sideways scattered angular distributions. Little change was seen between the perpendicular and parallel polarizations for the most forward laboratory angles, but the location of the peak shifted back substantially for the perpendicular result and showed a much larger contribution from angles behind the center of mass. Both ß = ± 45° alignment scans were intermediate between the parallel and perpendicular, with neither showing as large a contribution at back angles. The ß = +45° angular distribution showed greater wide angle scattering than the ß = -45°. The narrow angular distributions indicate that considerable energy remains in Br_2^- vibration.

Figure 4 shows a series of polarization scans of Ba^+ taken at a range of laboratory scattering angles for in-plane rotation of the p orbital. These were obtained by monitoring the Ba^+ flux at a given laboratory angle as a function of laser polarization. All scans are fit by the expression[32]

$$I(\beta) = \frac{(I_{max}+I_{min})}{2} + \frac{(I_{max}-I_{min})}{2}\cos 2(\beta-\beta').$$

The values of $(I_{max}-I_{min})/I_{min}$ and ß', the peak alignment angle, obtained from the fits are shown in Table 1. The alignment dependence is quite strong, reaching 1.2 at back angles, but varies significantly with angle and no clear trend appears. The location of the peak (ß') changes monotonically with scattering angle, almost through a full 180°, but the change at the back angles is much slower than at the forward angles.

The polarization scans of Figure 4 were scaled using the measured angular distributions to yield the alignment-angular distributions shown in Figure 5. Each grid point thus corresponds to a measured data point. The maximum flux occurred for ß=90°, perpendicular alignment of the p orbital with respect to the relative velocity vector, while the minimum appeared for parallel polarization.

B. Out-of-Plane Polarization Rotation

Figure 6 shows Ba^+ flux as a function of scattering angle and alignment angle for out-of-plane rotation of the p orbital. The widest laboratory angle accessible in this experimental geometry was 35°; beyond this the laser was obstructed by the detector. The out-of-plane polarization rotation-angular distribution result in Figure 6 shows the domination of in-plane alignment independent of laboratory angle, and again a peak

somewhat forward of the center-of-mass. There is no indication of the dramatic change of peak alignment angle with laboratory scattering angle which was observed for the in-plane orbital rotation experiments. Figure 7 shows the out-of-plane polarization scans unscaled by the angular distributions, in which the importance of in-plane alignment (θ = 90°) is quite clear. In addition, Figure 7 suggests a correlation between laboratory scattering angle and the magnitude of the alignment effect. The ratio $(I_{max}-I_{min})/I_{min}$ ranged from a minimum of 1 at 35°, to a maximum of 4 at 10°.

IV. DISCUSSION

Reaction of ground state barium with Br_2 at thermal energies is dominated by the production of the neutral radical pair BaBr and Br via the celebrated "harpoon mechanism".[32] Reaction is initiated with electron transfer from the metal atom to the halogen molecule at a distance at which the Coulomb interaction of the nascent ion pair compensates for the energy deficit of the electron transfer. Vertical electron attachment to Br_2 results in rapid stretching of the $(Br\text{-}Br)^-$ bond with subsequent dissociation in the field of the positive ion. Little momentum is transferred to the "spectator" bromine atom and forward scattered, vibrationally excited BaBr results.[33] Analogy with the extensively studied K-Br_2 system suggests that the neutral reaction dominates up to collision energies in the range 2-5 eV. At higher collision energies, formation of the ion pair M^+ and Br_2^- dominates and the cross section for neutral reaction products becomes negligible.[34]

Studies of ion pair formation in 5-1000 eV alkali metal-halogen molecule collisions have provided remarkable insight into the dynamics of these nonadiabatic processes. A generalized Landau-Zener treatment[35-40] gives the probability for remaining on a given adiabatic potential surface after passage through the crossing region:

$$p = 1-e^{-\delta}$$

where

$$\delta = \frac{2\pi H_{12}^2 R_c^2}{v}\left(1-\frac{b^2}{R_c^2}\right)^{-\frac{1}{2}}$$

in which v is the initial relative velocity, b the impact parameter and R_c the internuclear distance at the crossing point. For an atom-molecule collision, the coupling matrix element H_{12} may have a strong dependence on the angle ϕ between the molecular axis and the radius vector, largely as a consequence of the symmetries of the diabatic surfaces.[41]

Olson et al., have compiled a large number of measured and calculated coupling matrix elements for atom-atom systems to obtain a semi-empirical expression relating coupling matrix element to crossing distance:[42]

in atomic units, where

$$H_{12}^{*} = R_x^{*}\exp(-0.86R_x^{*})$$

$$H_{12}^{*} = \frac{H_{12}}{\sqrt{I_1 I_2}}$$

and

$$R_c^{*} = (\sqrt{I_1}+\sqrt{I_2})R_c$$

are the reduced coupling matrix element and reduced crossing distance, respectively, and I_1 and I_2 are the initial and final ionization potentials of the transferred electron. This expression yields values within a factor of three for >80% of the compiled data, over a range of 10 orders of magnitude of the reduced coupling matrix element. The semi-empirical coupling elements may be used with the Landau-Zener result above to examine the dependence of electron transfer probability on crossing distance and collision parameters. At low to moderate collision energies, exclusively adiabatic behavior is predicted for crossing distances below about 7 Å, with a very rapid transition to nonadiabatic behavior with increasing crossing distance. This is illustrated in Figure 8 for conditions relevant to the Ba-Br_2 system. The dependence of adiabatic transition probability on crossing distance is shown for reactions of Ba($^1P_1$), using an ionization potential of 3 eV, a relative velocity of 2000 m/s and impact parameter b = 0 and 10 Å, while the electron affinity is allowed to vary. Although the slopes are somewhat different, the general features of these curves are the same: the adiabatic transition probability falls rapidly in the region from 10 Å to 15 Å.

This exponential dependence of the coupling on the crossing distance yields the "bond-stretching" phenomenon which is perhaps the central feature of the dynamics of ion pair formation in alkali metal-halogen molecule collisions.[43] Following electron transfer on approach, the consequent stretching of the $(X\text{-}X)^-$ bond results in a substantial increase in the X_2 electron affinity, with a corresponding increase in the crossing distance and decrease in the coupling matrix element. As the molecular ion vibrates, the electron affinity varies considerably. The probability for electron transfer on exit may thus undergo oscillations, and in general will be very different from that on approach. Alternatively, nonadiabatic behavior on approach will lead to another opportunity for ion pair formation, in electron transfer on exit (the "covalent" trajectories). Because electron transfer on approach (the "ionic" trajectories) results in greater opportunity for the ion pair to experience the strong Coulomb attraction, the ionic trajectories in general will be deflected to larger scattering angles than the covalent trajectories.

The foregoing discussion derives largely from studies of ion pair formation in relatively high energy (5-1000 eV) collisions of ground state alkali atoms with halogen molecules. The nonadiabatic behavior in that case is largely a consequence of the high velocity through the crossing region. Nonadiabatic transitions are observed even though the crossing distances may be relatively small. The use of electronically excited atoms also promotes nonadiabatic behavior, but through effects on the coupling matrix elements directly since different potential energy surfaces are involved. Excitation of Ba to the (^{1}P) state results in a lowering of its ionization potential from 5.2 to 3.0 eV. This

moves the first crossing for the Ba-Br_2 system from ~4 Å to ~12 Å. As noted above, this is the region at which the coupling matrix element, hence the adiabatic transition probability, is dropping rapidly as a function of crossing distance. Another important effect of laser excitation on the coupling matrix element results from the change in the symmetries of the diabatic surfaces. The Ba(^{1}P)-Br_2 system actually represents three distinct potential energy surfaces, and their intersection with the $Ba^+(^2S)$-Br_2^- surface is schematically illustrated for $C_{\infty v}$ and C_{2v} geometries in Figure 9. This outer crossing represents a conical intersection[44,45] of the potential surfaces, and the coupling matrix elements are expected to show a ϕ dependence[46] given by:

$$(H_{12}(\phi))^2 = (H_{12}^o)^2\sin^2(\phi) \quad for\ p_x$$

$$(H_{12}(\phi))^2 = (H_{12}^o)^2\cos^2(\phi) \quad for\ p_z$$

$$(H_{12}(\phi))^2 = 0 \qquad for\ p_y.$$

The coupling matrix element, hence the probability of electron transfer, will thus be sensitive to alignment of the barium p orbital.

The Σ orbital alignment in $C_{\infty v}$ results in an avoided intersection at this outer crossing. In C_{2v} geometry this orbital alignment corresponds to A_1 symmetry, for which there is no interaction with the B_1 symmetry σ^* orbital of Br_2. The two favorable configurations for electron transfer are Σ in $C_{\infty v}$ and B_1 in C_{2v}. One may thus use the

orbital alignment dependence of the cross sections for different reaction channels to make inferences about the important nuclear geometries, and this is the basis of the argument presented by Rettner and Zare for their $Ca(^1P_1)$ + Cl_2 alignment dependence.[27] But to make sense of alignment effects, the relation between the asymptotically prepared orbital alignment and the geometry of the collision complex must be divined. For head-on collisions there is no ambiguity, but for finite impact parameter collisions an initially prepared Σ state may evolve into either a Σ or Π state of the collision complex, depending on the magnitude of the splitting between the Σ and Π potential energy curves: that is, depending on whether Ω is a good quantum number for the system. This is the orbital locking phenomenon, the importance of which is now universally recognized.[47,48] In atom-atom scattering there exists both experimental and theoretical evidence for a "locking radius" at which point the body-fixed reference frame becomes the important one.[49,50] An analogous phenomenon is anticipated in atom-molecule collisions, although greatly complicated by the additional nuclear degrees of freedom and the anisotropy of the potential. Rettner and Zare argued that the alignment dependence observed for all products studied in the $Ca(^1P_1)$-Cl_2 reaction indicated the importance of electron transfer at the outer crossing region, and this is entirely consistent with our observations in the present study. In addition, they inferred from the fact that all channels were favored by Π alignment that broadside collisions were dominant and orbital following was perhaps important. Simons, in a 1987 review[51], hinted that the $Ca(^1P_1)$-Cl_2 results might alternatively be understood to result from large impact parameter collisions which are outside the locking radius for the system. Our

results are clearly in accord with Simons' remark, and they suggest the model illustrated in Figure 10. Three conclusions serve to rationalize all the experimental findings: 1) The crossing point is beyond the locking radius for the system; 2) The charge transfer process is dominated by large impact parameter collisions, for which asymptotic Π alignment corresponds to Σ alignment in the body fixed frame at the crossing point; and 3) The internuclear geometry is collinear at the critical configuration.

We first consider alignment dependence of charge transfer in $Ba(^1P_1)$-Br_2 collisions for in-plane rotation of the p orbital. If one assumes initial and final nuclear orbital angular momentum vectors to be parallel, a reasonable approximation here, then both configurations favoring electron transfer, Σ in $C_{\infty v}$ and Π in C_{2v}, require the impact parameter to lie in the scattering plane. All Ba^+ will be scattered in the scattering plane (the plane of the detector) regardless of alignment angle. This is also consistent with the results for the $Ca(^1P_1)$-Cl_2 discussed above, in which there was no scattering plane to break the cylindrical symmetry of the experiment. Several aspects of the data indicate that large impact parameter collisions dominate the production of the charge transfer process. All Ba^+ is forward or forward-sideways scattered, as expected for large impact parameter collisions. The different angular distributions for $\beta = \pm 45°$, shown in Figure 3, can be readily understood as a consequence of a negative correlation between impact parameter and scattering angle. Most importantly, the different nature of the alignment dependence for in-plane and out-of-plane polarization scans strongly suggests the dominance of large impact parameter collisions.

The out-of-plane results shown in Figures 6 and 7 enable us to determine the relative importance of C_{2v} and $C_{\infty v}$ geometries. The alignment dependence is always favored for collisions in which the orbital lies in the scattering plane. If C_{2v} (broadside) geometries were dominant, then one would expect little alignment dependence for out-of-plane rotation. There is as likely to be a suitably oriented Br_2 molecule whether or not the p orbital is in the scattering plane. If collinear geometry were dominant, however, dramatic alignment effects might be anticipated. Although perpendicular orbital alignment is most favorable for electron transfer, for out-of-plane orbital alignment this would occur only for impact parameters lying in a plane perpendicular to the scattering plane: most products would thus scatter out of the plane containing the detector. Figures 5 and 6 together thus strongly suggest that large impact parameter collisions which achieve a collinear nuclear configuration and Σ orbital alignment at the crossing point dominate this process.

These conclusions find further support in the angular distributions of figure 3. The increased flux seen for perpendicular over parallel polarization appears to be less forward scattered. This is consistent with preliminary translational energy scans which suggest that perpendicular alignment leads to an increase in the sideways scattered product. These distributions may be understood with recourse to figure 10. The perpendicular alignment favors electron transfer for the large impact parameter collisions. These will not necessarily lead to forward scattering, however. The long-range coulomb interaction may still produce significant deflection even in these collisions. As mentioned above, the most forward scattered flux will be that which

originates from covalent trajectories: those for which electron transfer occurs on exit rather than on approach.[43] Parallel alignment favors lower impact parameter collisions. In this case, electron transfer on approach results in a strong interaction which probably favors neutral products or the chemiion channel.[28,45] The charge transfer channel may only be possible for low impact parameter collisions via the covalent trajectories. Parallel alignment thus produces the most forward scattered flux. The ß = ±45° results further indicate that for these still relatively large impact parameter collisions (b = 10/$\sqrt{2}$ = 7 Å), electron transfer occurs on approach rather than on exit. For ß = +45°, the tendency to wide angle scattering reveals that this orbital alignment favors positive center of mass scattering angles. The more forward laboratory angular distribution for ß = -45° indicates that this results in scattering into negative center of mass angles, as illustrated schematically in Figure 11. The dramatic change of ß' with laboratory scattering angle seen in the scans of Figure 4 and Table 1, actually maps the impact parameter dependence of the reaction.

Orbital locking is expected when Ω-splitting of the potentials is large relative to the angular velocity of the collision. This Ω-splitting may be expressed as a precession frequency of the electronic orbital angular momentum vector about the internuclear axis[52]:

$$\omega_{prec}(R) = \Delta V(R)/\hbar \ .$$

The condition for orbital locking then becomes:

$$\omega_{prec}(R) >> \dot{\phi}(R) \ ,$$

where $\dot{\phi}(R)$ is the angular velocity of the collision. A "locking radius", R_L, may be defined at some internuclear distance smaller than which this condition is considered to hold. Manders et al., in semi-classical trajectory studies of alignment effects in Ne**-Ar collisions, have found the condition

$$\omega_{prec}(R_L) = 4\dot{\phi}(R_L)$$

provides a reasonable definition for this locking radius.[53] Applying these considerations we can estimate the magnitude of Ω-splitting necessary to induce orbital locking in the $Ba(^1P_1)$-Br_2 system. For an impact parameter of $R_c/\sqrt{2}$ = 7Å, the splitting between the potentials would have to exceed 4 meV at 10Å in order for orbital locking to be possible there. Splitting of this magnitude seems unlikely at such long range. Although the discussion is strictly appropriate only for atom-atom collisions, it is useful to provide a sense for the magnitude of the forces involved, and is unlikely to be seriously in error at the large Ba-Br_2 distances considered.

From the foregoing discussion we might not anticipate orbital locking to be important for this system. Indeed, although they do not preclude the possibility of orbital locking, the experimental results argue the importance of the space fixed reference frame throughout the collision. The observed Π alignment dependence implies that for these dominant geometries, the laboratory-prepared orbital alignment is precisely that which is relevant in the collision. If this were not the case, we would anticipate a dominant orbital alignment somewhat shifted from perpendicular, which could evolve to the favorable geometry through rotation of the molecule fixed frame as the internuclear distance changed from R_L to R_C.

The narrow angular distributions in Figure 3 are consistent with the limited energy available to translation following electron attachment to Br_2. The inner circle represents the maximum Ba^+ velocity based on the vertical electron affinity of Br_2: ion pair production via vertical electron attachment is 1.4 eV endoergic. Most of the distribution falls within this limiting circle. This Ba^+ production following vertical electron attachment requires effective coupling of the initial translational energy into the reaction coordinate. Yet for the dominant large impact parameter collisions the radial velocity (the reaction coordinate) may be very small at the moment of electron transfer. Moreover, similar results were obtained at 1 eV collision energy, yet this is below the endoergicity of the process for a simple vertical electron transfer. Several alternatives may be considered to account for this apparent discrepancy. Ion pair production is consistently observed in alkali-halogen molecule collisions below thresholds based on the vertical electron affinities: in fact thresholds for ion pair production yield good values for the adiabatic electron affinities of halogen molecules.[54] This results from "prestretching" of the halogen bond in the presence of the alkali atom, and it has been shown to be important even up to collision energies of 120 eV.[43,55] Yet prestretching may be less important at the large distances considered here. Alternatively, although the vertical electron affinity of Br_2 is given as 1.6 eV, owing to the steepness of the Br_2^- potential in this region the Franck-Condon envelope is >0.8 eV wide, so a broad range of Br_2^- vibrational states may be reached. Furthermore, the low vibrational frequency of Br_2 (325 cm^{-1}) implies a substantial vibrationally excited population. Under the conditions of our experiment and assuming no vibrational relaxation in the supersonic expansion,

>20% of the Br_2 is in v=1. For Br_2 (v=1), vertical electron transfer may reach deep into the Br_2^- well, resulting in the release of considerably more energy to the reaction coordinate. All of the foregoing considerations are probably relevant and classical trajectory calculations would be useful to address these questions.

It is interesting to note that in the $Ca(^1P)$-Cl_2 system studied by Rettner and Zare, and the Na(4D)-O_2 and $Ba(^1P)$-Br_2 studies from our laboratory, the conditions were such that adiabatic transition probability, as given by the Landau-Zener treatment discussed above, was significantly different from both one and zero. That is, the experiments were performed in the region in which the coupling varies rapidly as a function of crossing distance (and in which its dependence on orbital alignment may have some measurable effect). Furthermore, in all these examples of strong alignment effects for reactive scattering, it is in nonadiabatic channels that these alignment effects are observed. In these channels the dominant adiabatic flux contributes no background. This suggests a general prescription for those seeking to exploit orbital alignment effects in the study of reactive scattering: 1) choose systems in which the adiabatic transition probability is changing rapidly as a function of crossing distance, and 2) study the nonadiabatic channels in these systems.

D. CONCLUSION

A strong dependence of the charge transfer cross section on orbital alignment was used to explore the stereochemical requirements of the initial electron transfer in

$Ba(^1P_1)$-Br_2 collisions. The orbital alignment dependence observed for Ba^+ production is striking in several respects. The magnitude of the effect, reaching $(I_{max}-I_{min})/I_{min} = 4$, is unprecedented in studies of atom-molecule scattering, particularly for reactive processes. In addition, the continuous change of the location of the polarization peak with scattering angle suggests important changes of impact parameter or nuclear geometry with alignment angle. Finally, there is an apparent contradiction between the in-plane result, which shows a maximum for perpendicular orbital alignment, and the out-of-plane result, which shows a minimum for perpendicular orbital alignment. These differences in the alignment dependence for in-plane and out-of-plane rotation of the barium p orbital indicate that the reaction is dominated by large impact parameter collisions for which the perpendicular orbital alignment corresponds to a Σ state in the molecular reference frame at the critical configuration.

Acknowledgement

This work was supported the Director, Office of Energy Research, Office of Basic Energy Sciences, Chemical Sciences Division, of the U.S. Department of Energy under Contract No. DE-AC03-76SF00098. AGS thanks Dr. M. H. Covinsky for helpful discussions and acknowledges the NSF for a graduate fellowship.
HFD thanks NSERC (Canada) for a 1967 Science and Engineering fellowship.

References

1. J. M. Parson, T. P. Schaefer, F. P. Tully, P. E. Siska, Y. C. Wong and Y. T. Lee, J. Chem. Phys. **53**, 2123 (1970).
2. P. E. Siska, J. M. Parson, T. P. Schaefer, F. P. Tully, Y. C. Wong and Y. T. Lee, Phys. Rev. Lett., **25**, 271 (1970).
3. H. Pauly and J. P. Toennies, Adv. At. Mol. Phys. **1**, 195 (1965).
4. F. P. Tully and Y. T. Lee, J. Chem. Phys. **57**, 866 (1972).
5. R. Schinke and J. Bowman, in **Molecular Collisions Dynamics**, (Springer-Verlag, Berlin, 1983).
6. P. L. Jones, U. Hefter, A. Mattheus, J. Witt, K. Bergmann, W. Muller,W. Meyer and R. Schinke, Phys. Rev. Lett. **46**, 915 (1981).
7. D. R. Herschbach, Disc. Faraday Soc., **33**, 149 (1962).
8. W. B. Miller, S. A. Safron and D. R. Herschbach, Disc. Faraday Soc., **44**, 292 (1967).
9. R. E. Minturn, S. Datz and R. L. Becker, J. Chem. Phys. **44** 1149 (1966).
10. I. V. Hertel and W. Stoll, Adv. At. Mol. Phys. **13**, 113 (1978).
11. D. H. Parker, H. Jalink, and S. Stolte, J. Phys. Chem. **91**, 5427 (1987).
12. I. V. Hertel, Adv. Chem. Phys. **45**, 341 (1981).
13. E. E. Nikitin, J. Chem. Phys. **43**, 744 (1965).

14. E. E. B. Campbell, H. Schmidt and I. V. Hertel, Adv. Chem. Phys. **72**, 37 (1988).

15. R. Duren, H. O. Hoppe, and H. Pauly, Phys. Rev. Lett. **37**, 743 (1976).

16. L. Huwel, J. Maier, R. K. B. Helbing and H. Pauly, Chem. Phys. Lett. **74**, 459 (1980).

17. L. Huwel, J. Maier and H. Pauly, J. Chem. Phys. **76**, 4961 (1982).

18. A. Fischer and I. V. Hertel, Z. Phys. A **304**, 103 (1982).

19. W. Reiland, G. Jameison, U. Tittes and I. V. Hertel, Z. Phys. A **307**, 51 (1982).

20. A. Bahring, I. V. Hertel and H. Schmidt, Z. Phys. A **320**, 141 (1985).

21. M. O. Hale, I. V. Hertel and S. R. Leone, Phys. Rev. Lett. **53**, 2296 (1984).

22. W. Bussert, D. Neuschafer and S. R. Leone, J. Chem. Phys. **87**, 3833 (1987).

23. W. Bussert and S. R. Leone, Chem. Phys. Lett. **138**, 269 (1987)

24. W. Bussert and S. R. Leone, Chem. Phys. Lett. **138**, 276 (1987).

25. P. S. Weiss, M. H. Covinsky H. Schmidt, B. A. Balko, Y. T. Lee and J. M. Mestdagh, Z. Phys. D **10**, 227 (1988).

26. H. Schmidt, P. S. Weiss, J. M. Mestdagh, M. H. Covinsky and Y. T. Lee, Chem. Phys. Lett. **118**, 539 (1985).

27. C. Rettner and R. N. Zare, J. Chem. Phys. **77**, 2416 (1982).

28. A. G. Suits, H. Hou and Y. T. Lee, J. Phys. Chem. **94**, 5672 (1990).

29. Y. T. Lee, J. D. McDonald, P. R. LeBreton and D. R. Herschbach, Rev. Sci. Instr. **40**, 1402 (1969).

30. P. E. Siska, J. M. Parson, T. P. Schaefer and Y. T. Lee, J. Chem. Phys. **55**, 5762 (1971).

31. H. F. Davis, M. H. Covinsky, A. G. Suits and Y. T. Lee, manuscript in preparation.

32. J. A. Haberman, K. G. Anlauf, R. B. Bernstein and F. J. Van Itallie, Chem. Phys. Lett., **16**, 442 (1972).

33. Shen-Maw Lin, Charles A. Mims, and Ronald R. Herm, J. Chem. Phys. **58**, 327 (1973).

34. C. W. A. Evers, Chem. Phys. **30**, 27 (1978).

35. L. D. Landau, J. Phys. (USSR) **2**, 46 (1932).

36. C. Zener, Proc. Roy. Soc. (London) **A137**, 696 (1932).

37. E. E. Nikitin, Opt. Spectrosc. **11**, 246 (1961).

38. R. K. Janev, Adv. At. Mol. Phys. **12**, 1 (1976).

39. Y. N. Demkov, Sov. Phys. JETP **18**, 138 (1964).

40. D. Rapp and W. E. Francis, J. Chem. Phys. **37**, 2631 (1962).

41. E. A. Gislason and J. G. Sachs, J. Chem. Phys. **62**, 2678 (975).

42. R. E. Olson, F. T. Smith and E. Bauer, Appl. Optics, **10**, 1848 (1971).

43. J. Los and A. W. Kleyn, in **Alkali Halide Vapors**, 189 (Academic Press, New York, 1979) and references.

44. G. Herzberg, **Electronic Spectra of Polyatomic Molecules** (Van Nostrand, Princeton NJ 1967).

45. Michael Menzinger, The M + X_2 Reactions: A Case Study, in **Gas Phase Chemiluminescence and Chemi-Ionization**, A. Fontijn, ed., Elsevier Science Publishers, B.V., 1985, pp.25-66.

46. E. E. Nikitin, Chem. Phys. Lett. **1**, 266 (1967).

47. G. C. Schatz, L. J. Kovalenko and S. R. Leone, J. Chem. Phys. **91**, 6961, (1989).

48. B. Pouilly and M. H. Alexander, Chem. Phys. **145**, 191 (1990).

49. L. J. Kovalenko, S. R. Leone and J. B. Delos, J. Chem. Phys. **91**, 6948 (1989).

50. J. P. J Driessen, Ph.D. Thesis, Eindhoven University (1989).

51. J. P. Simons, J. Phys. Chem. **91**, 5378 (1987).

52. J. P. J. Driessen, F. J. M. v. d. Weijer, M. J. Zonneveld, L. M. T. Somers, M. F. M. Janssens, H. C. W. Beijerinck and B. J. Verhaar, Phys. Rev. Lett., **62**, 2369 (1989).

53. M. P. I. Manders, W. B. M. van Hoek, E. J. D. Vredenbregt, G. J. Sandker, H. C. W. Beijerinck and B. J. Verhaar, Phys. Rev. A **39**, 4467 (1989).

54. A. P. M. Baede, D. J. Auerbach and J. Los, Physica **64**, 134 (1973).

55. J. A. Aten and J. Los, Chem. Phys. **25**, 47 (1977).

Table 1: Ba^+ In-Plane Alignment Dependence

Lab Angle	$(I_{max}-I_{min})/I_{min}$	ß'
10.0°	.89	35°
12.5°	.91	23°
15.0°	.71	16°
17.5°	.41	1°
20.0°	.27	159°
22.5°	.27	137°
25.0°	.35	120°
27.5°	.46	111°
30.0°	.52	105°
32.5°	.68	100°
35.0°	.85	93°
37.5°	.95	89°
40.0°	1.06	85°
42.5°	1.23	82°
45.0°	1.25	77°
47.5°	.19	72°
50.0°	.94	66°
52.5°	.70	59°
55.0°	.53	56°
57.5°	.50	52°
60.0°	.44	57°

Table 1: Ba^+ alignment dependence for in-plane orbital rotation. Values of $(I_{max}-I_{min})/I_{min}$ and ß' were obtained from the fits shown in Figure 4.

Figure Captions

Fig. 1. (A) Schematic view of crossed beams apparatus at interaction region showing modifications for detection of ions. (B) Experimental geometry for in-plane rotation of barium p orbital. (C) Experimental geometry for out-of-plane rotation of p orbital.

Fig. 2. Schematic illustration of orbital alignment geometry for (A) in-plane and (B) out-of-plane rotation of the barium p orbital.

Fig. 3. Laboratory angular distributions of Ba^+ from the reaction $Ba(^1P_1)$ + $Br_2 \rightarrow Ba^+ + Br_2^-$ at 1.6 eV collision energy shown with the nominal Newton diagram. The orbital alignment was ß = 90°(circles), 0°(diamonds), -45°(squares) or +45°(triangles). The solid and dashed circles represent maximum Ba^+ recoil velocity based on adiabatic and vertical Br_2 electron affinities, respectively.

Fig. 4. Experimental polarization dependences of Ba^+ at a collision energy of 1.6 eV for in-plane rotation of the barium p orbital at the indicated laboratory angles. Beta is the angle of the polarization with respect to the relative velocity vector. Also shown is a typical example of the $Ba(^1P_1)$ fluorescence intensity, which was monitored simultaneously for all scans.

Fig. 5. The data of Figure 4 scaled by the angular distributions of Figure 3 to yield a polarization-laboratory angular distribution.

Fig. 6. Experimental polarization-laboratory angular distribution of Ba^+ at a collision energy of 1.6 eV for out-of-plane rotation of the barium p orbital. The polarization angle, θ, is taken to be zero when the laser polarization is perpendicular to the scattering plane.

Fig. 7. The data of Figure 6 scaled so that the polarization maxima at each laboratory angle are equal.

Fig. 8. Adiabatic transition probability calculated as described for $Ba(^1P_1)$ collisions at a relative velocity of 2000 m/s and impact parameter b = 0 Å (solid line) or b = 10 Å (dotted line).

Fig. 9. Schematic illustration of possible reaction geometries (adapted from Ref. 45).

Fig. 10. Model illustrating important orbital alignment at the outer crossing for the $Ba(^1P_1)$-Br_2 charge transfer reaction.

Fig. 11. Qualitative illustration of different laboratory scattering angles for $\beta = \pm 45°$ orbital alignment.

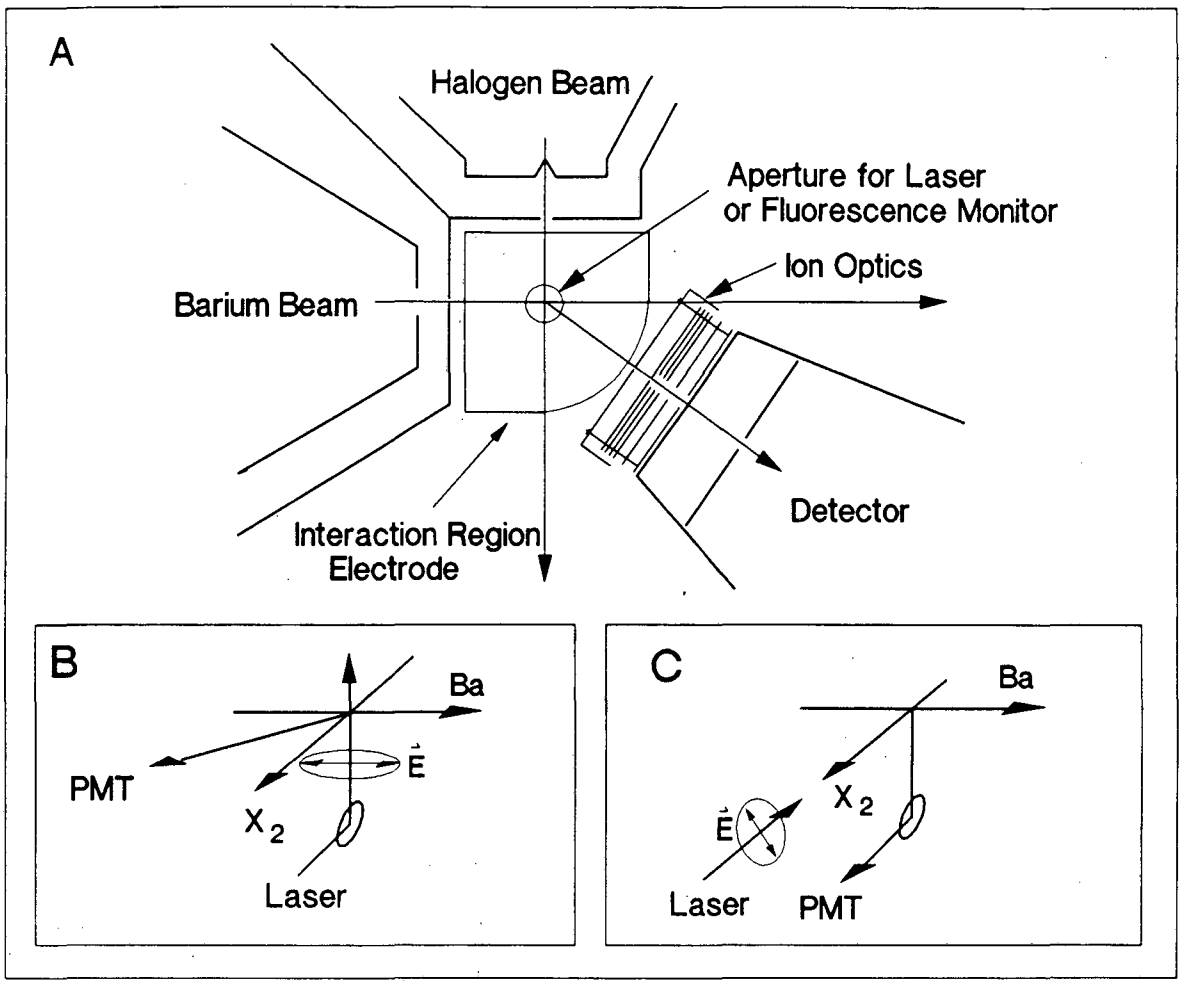
A
Halogen Beam
Aperture for Laser
or Fluorescence Monitor
Ion Optics
Barium Beam
Detector
Interaction Region
Electrode
B
Ba
PMT
$\vec{E}$
X_2
Laser
C
Ba
X_2
$\vec{E}$
Laser
PMT

Figure 1

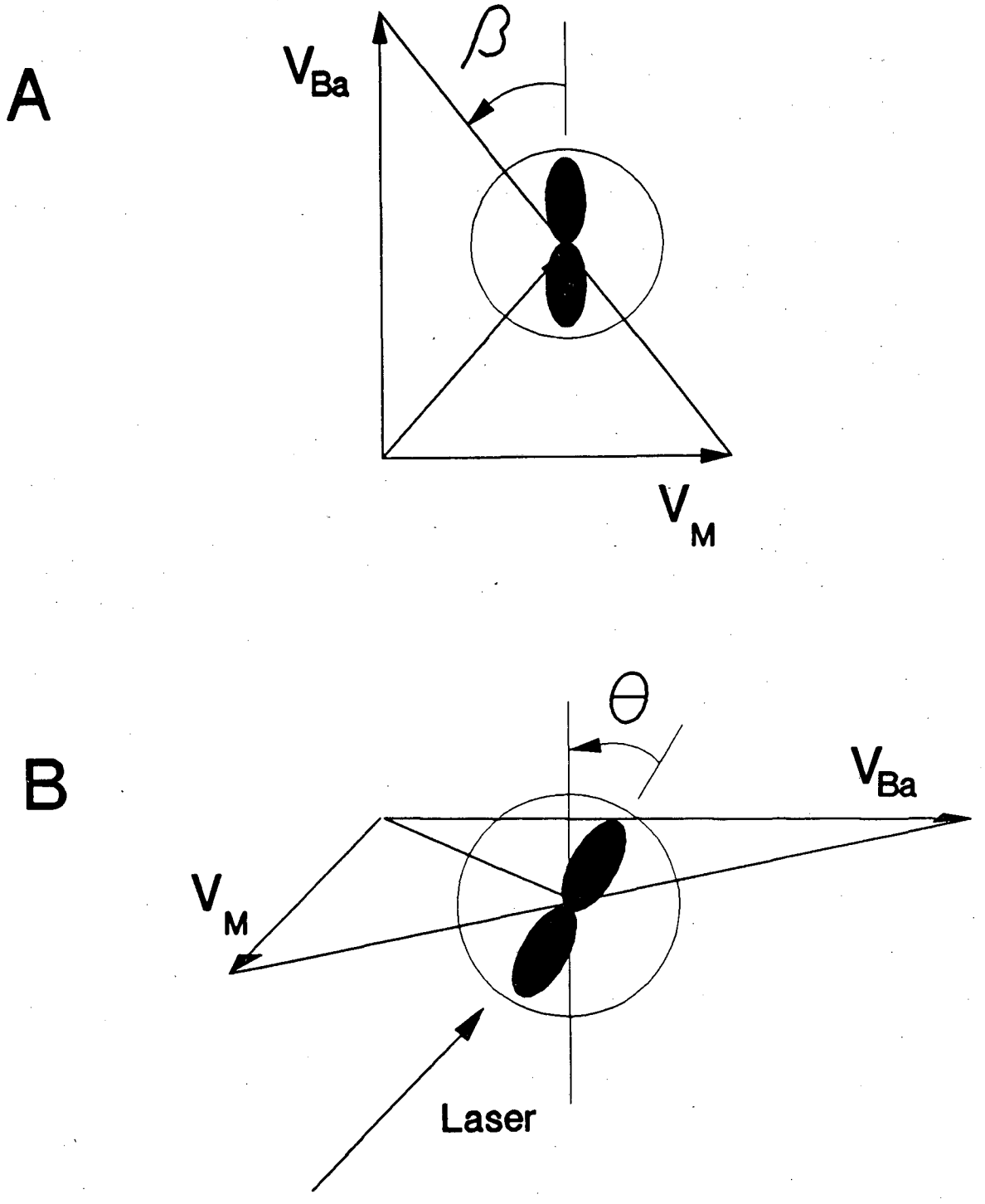

XBL 916-1271

Figure 2

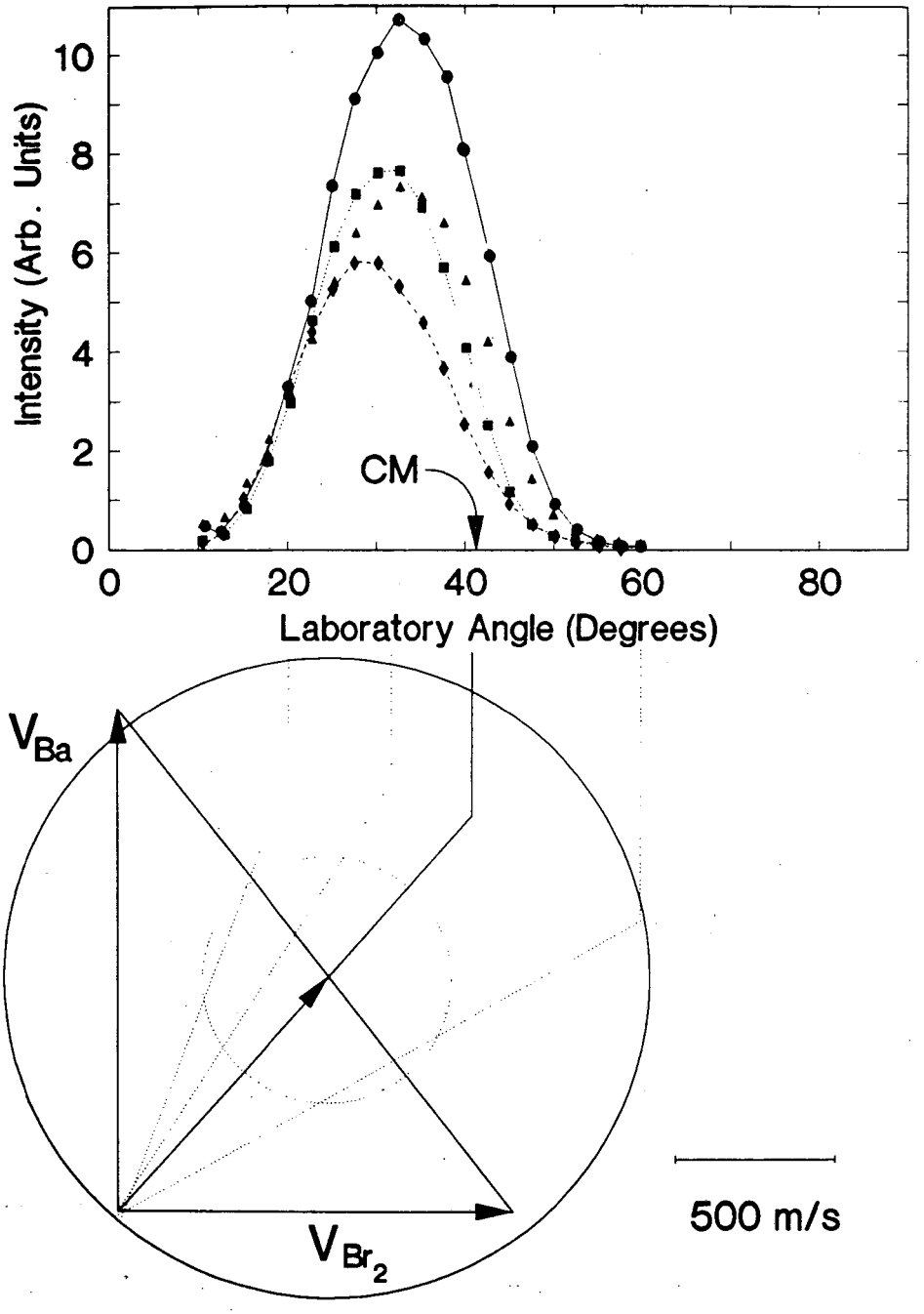
Intensity (Arb. Units)
10
8
6
4
2
0
0
20
40
60
80
CM
Laboratory Angle (Degrees)
V_{Ba}
V_{Br_2}
500 m/s
XBL 916-1270

Figure 3

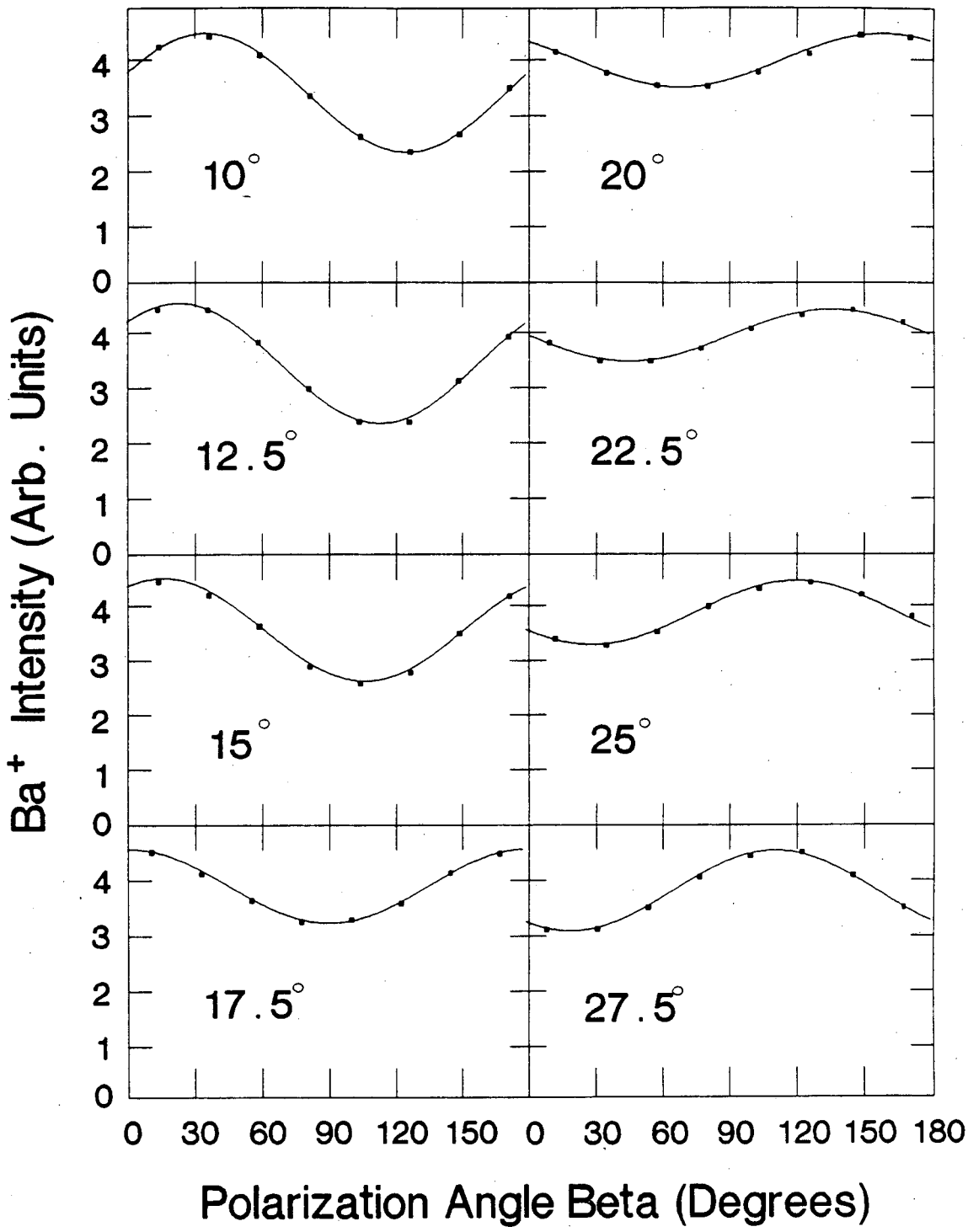

XBL 916-1193

Figure 4(a)

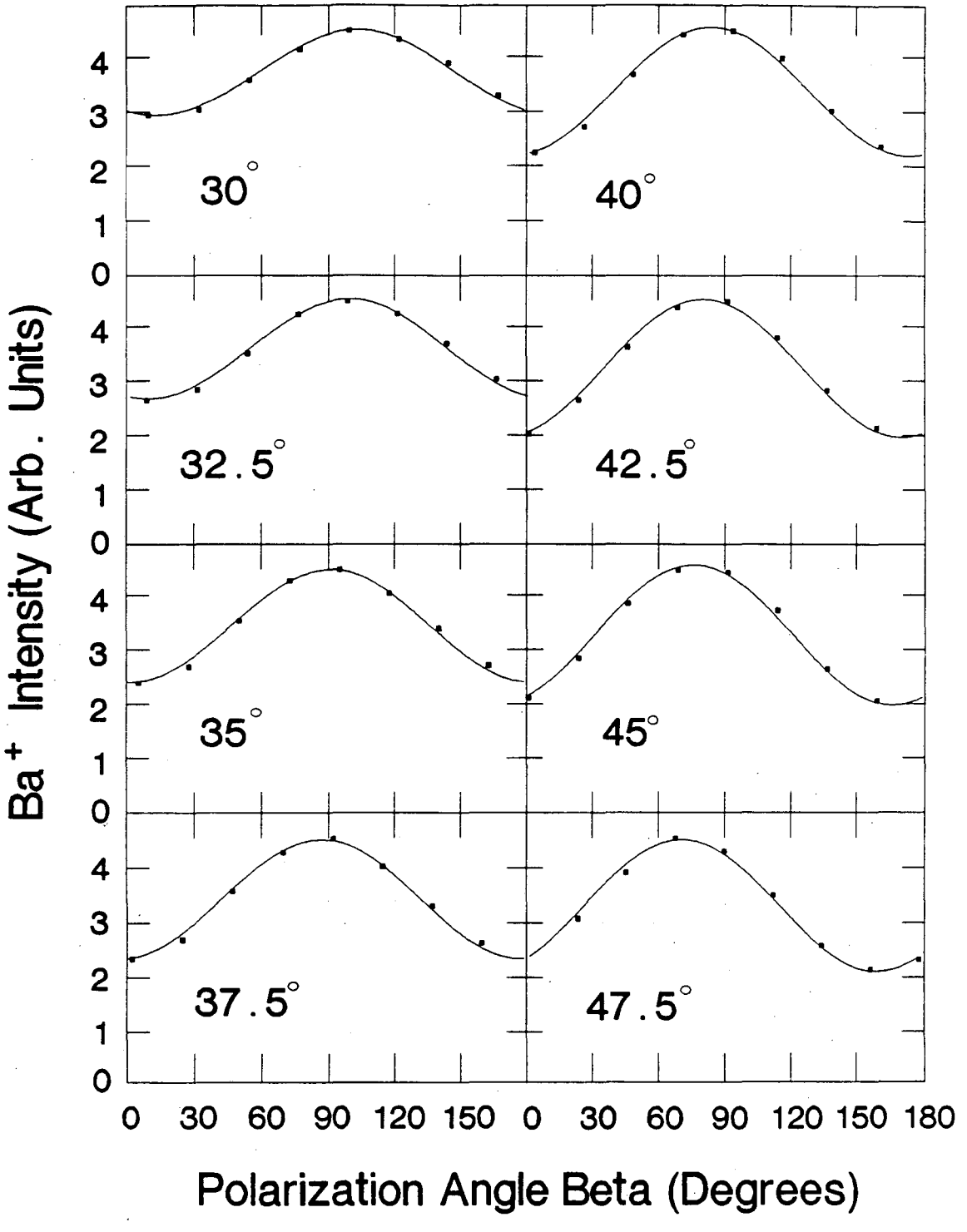

XBL 916-1194

Figure 4(b)

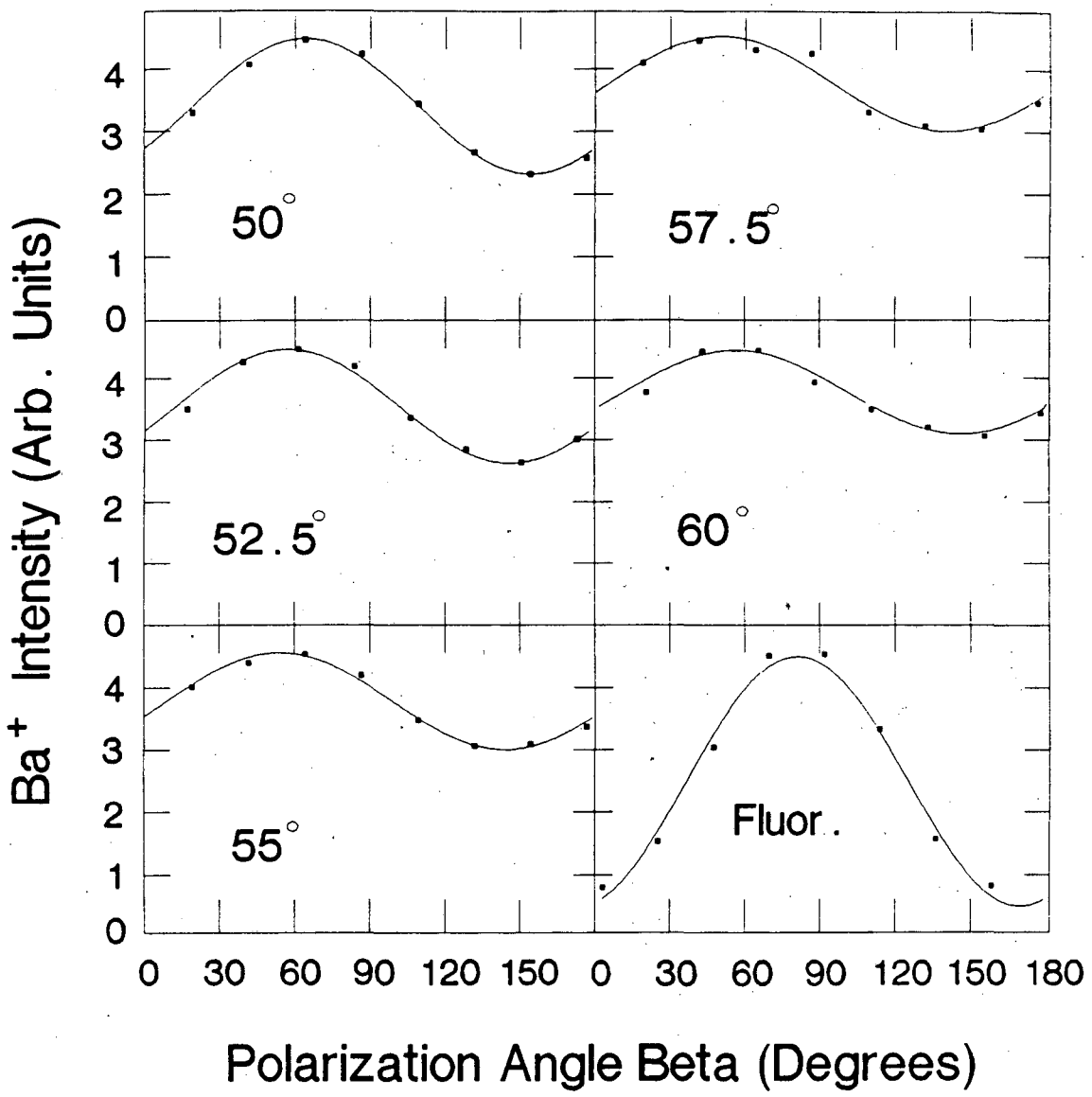

XBL 916-1195

Figure 4(c)

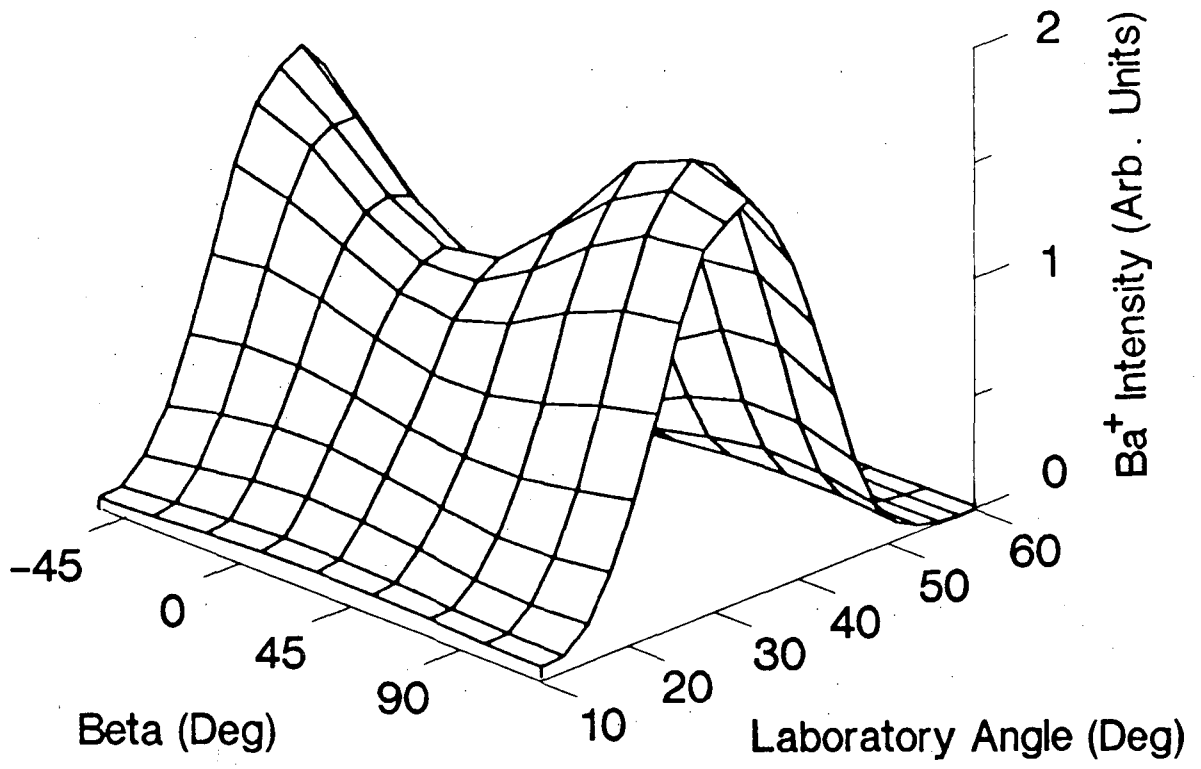
2
1
0
Ba+ Intensity (Arb. Units)
-45
0
45
90
Beta (Deg)
10
20
30
40
50
60
Laboratory Angle (Deg)

Figure 5

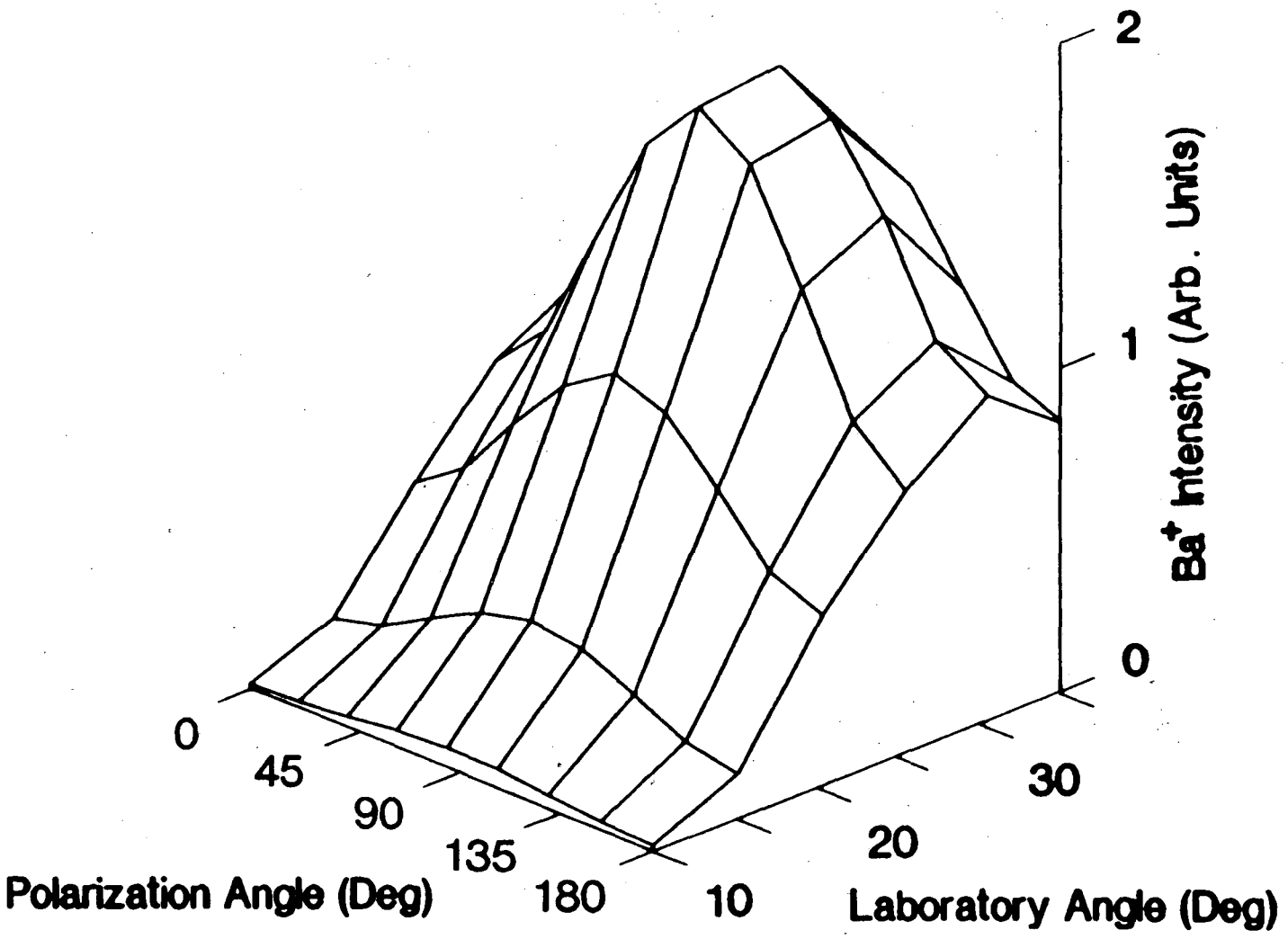

Figure 6

XBL 916-1196

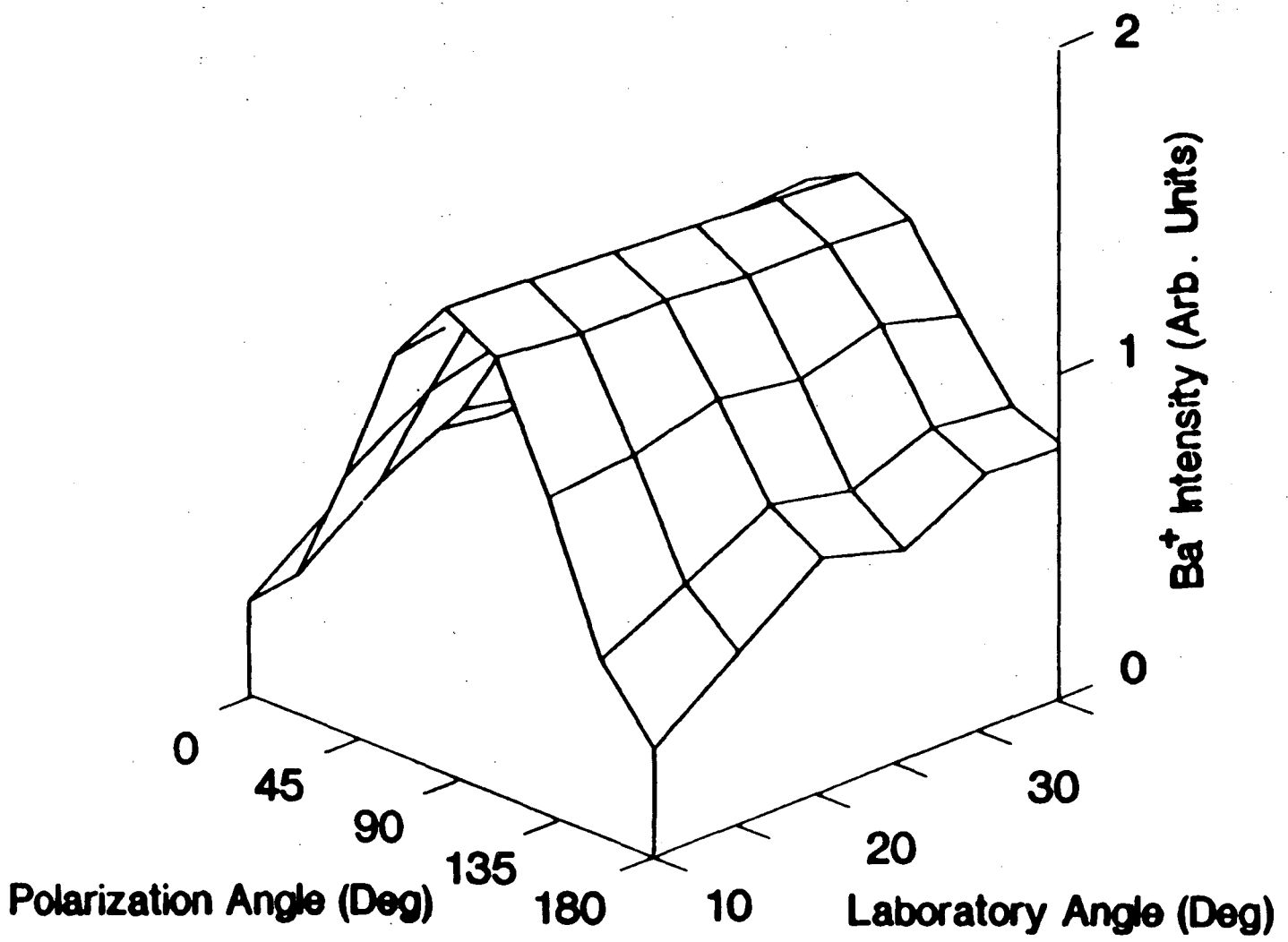

Figure 7

XBL 916-1197

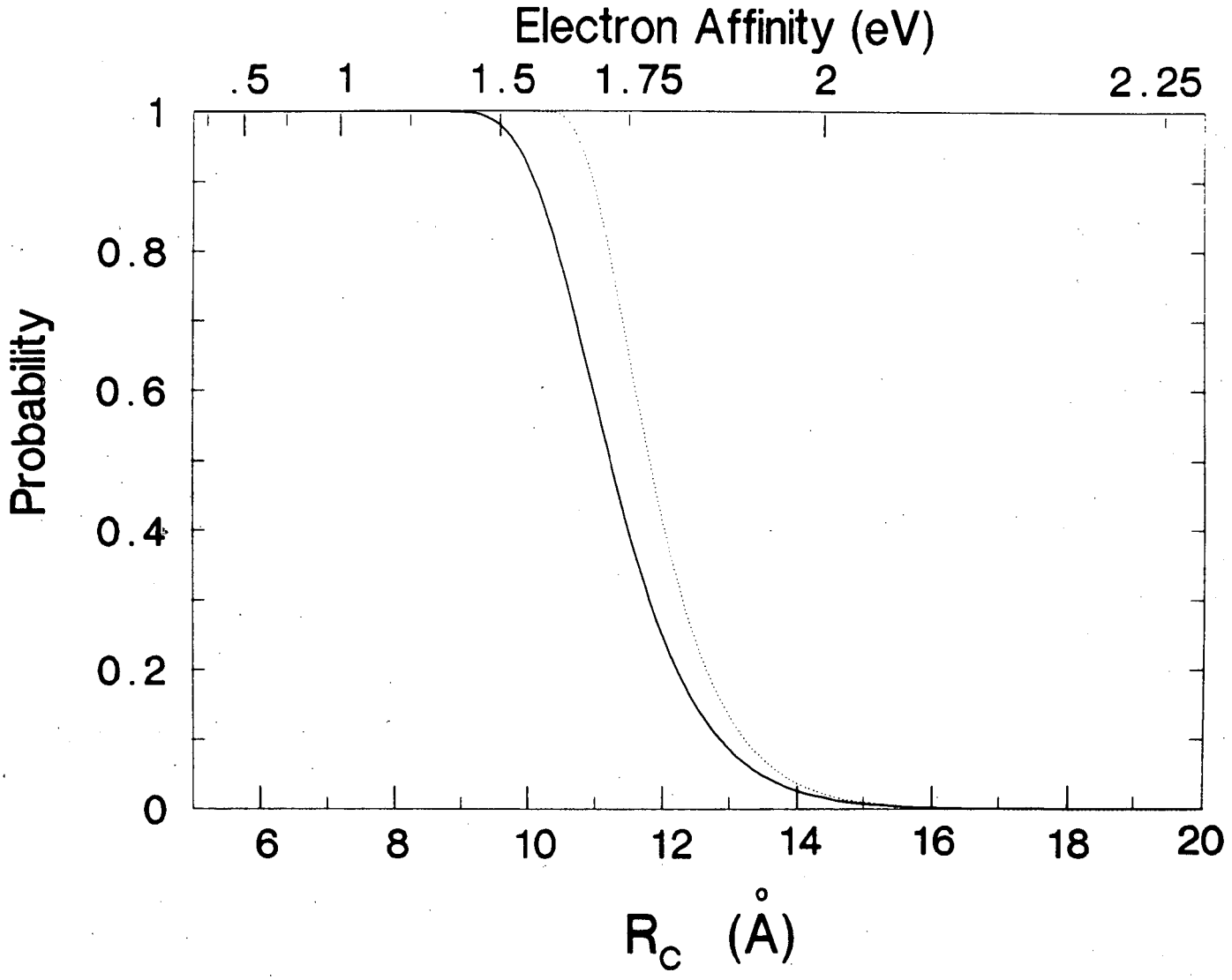

Figure 8

XBL 916-1272

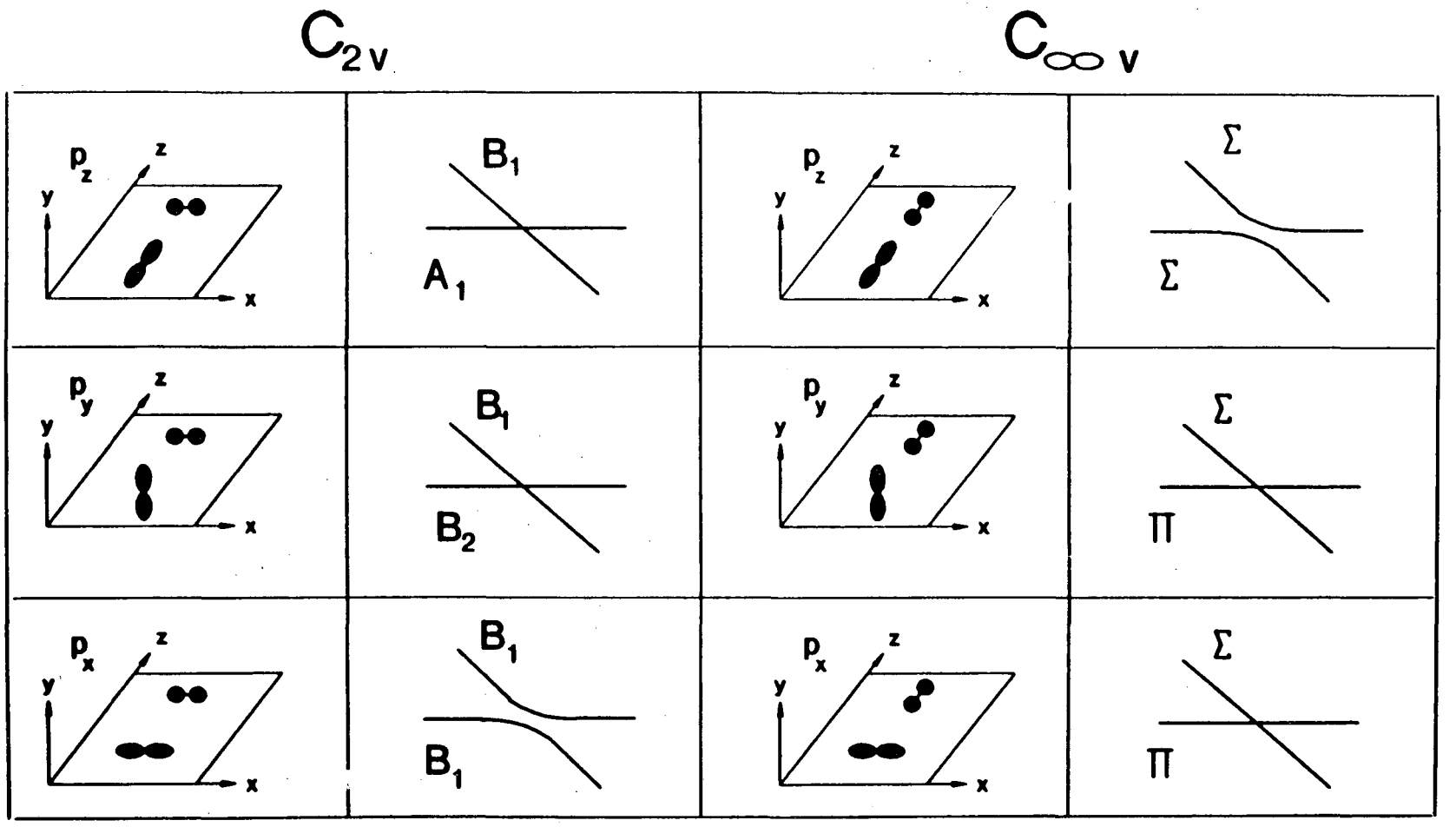

Figure 9b

XBL 916-1273

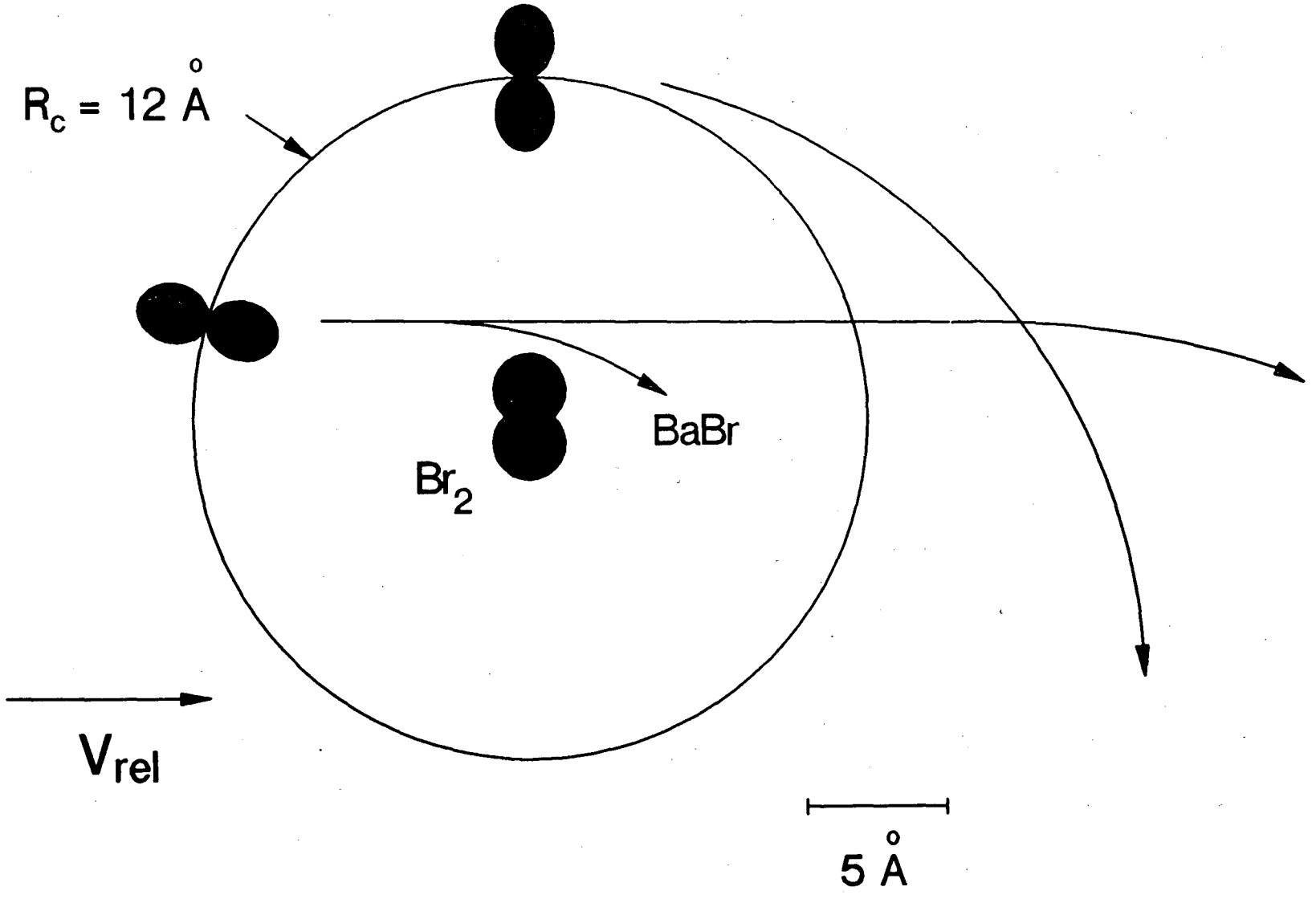

Figure 10

XBL 916-1269

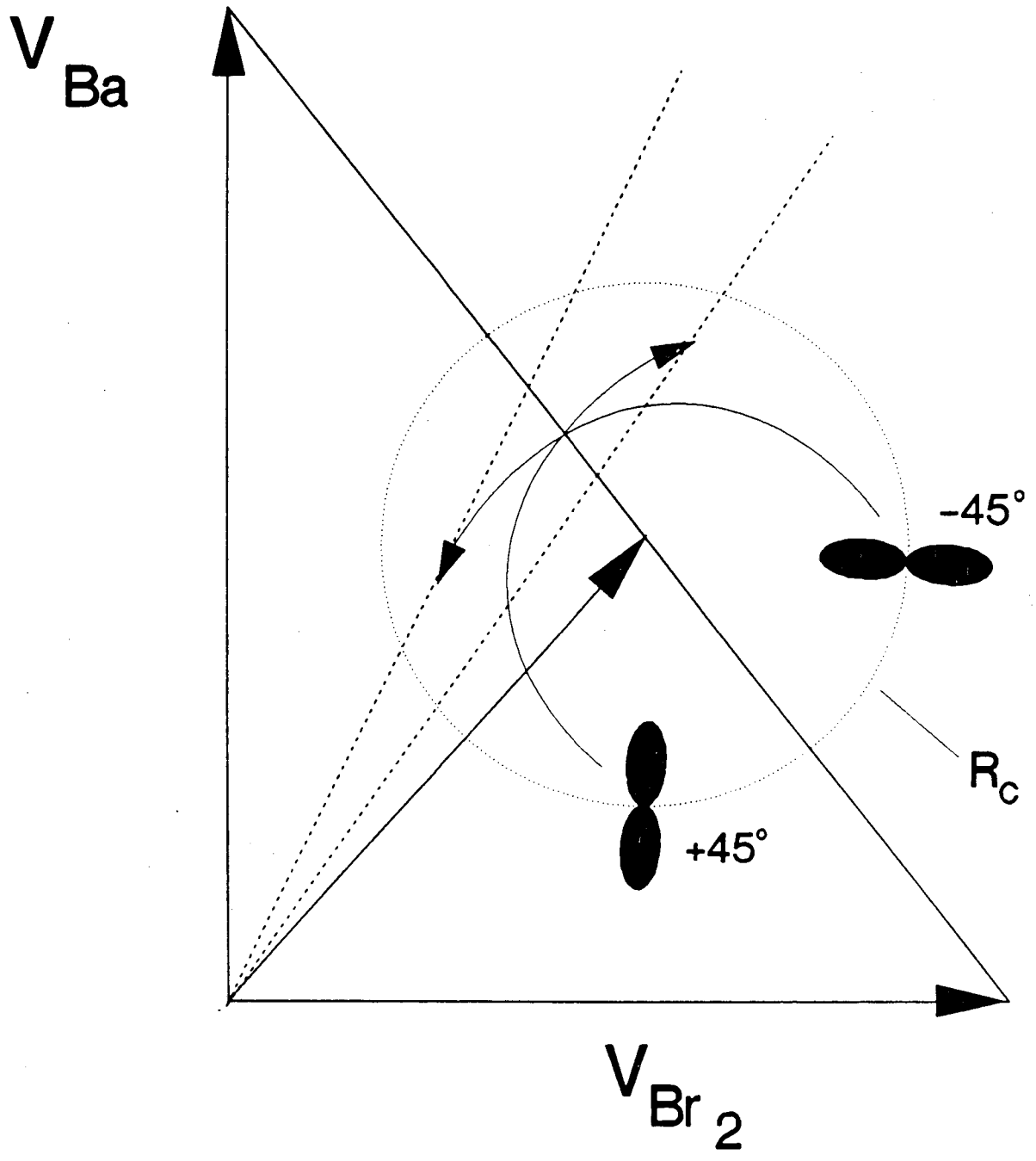

Figure 11 XBL 916-1274

LAWRENCE BERKELEY LABORATORY
UNIVERSITY OF CALIFORNIA
INFORMATION RESOURCES DEPARTMENT
BERKELEY, CALIFORNIA 94720